Applied Catalysis B: Environmental 142–143 (2013) 290–297

Contents lists available at SciVerse ScienceDirect

Applied Catalysis B: Environmental

journal homepage: www.elsevier.com/locate/apcatb

Relationship between structure and performance of a novel cerium-niobium binary oxide catalyst for selective catalytic reduction of NO with NH_3

Ruiyang Qu[a,b], Xiang Gao[a,*], Kefa Cen[a], Junhua Li[b,**]

[a] State Key Laboratory of Clean Energy Utilization, Department of Energy Engineering, Zhejiang University, Hangzhou 310027, China
[b] State Key Joint Laboratory of Environment Simulation and Pollution Control, School of Environment, Tsinghua University, Beijing 100084, China

ARTICLE INFO

Article history:
Received 13 March 2013
Received in revised form 14 May 2013
Accepted 16 May 2013
Available online 23 May 2013

Keywords:
$DeNO_x$
Selective catalytic reduction
Ce-Nb catalysts
Short-range activation effect

ABSTRACT

A series of Ce-Nb binary oxide catalysts for the selective catalytic reduction (SCR) of NO with ammonia were synthesized using co-precipitation method and showed good catalytic activity and selectivity. The best catalyst Ce1Nb1 presented over 80% NO conversion in a wide temperature range of 200–450 °C at a gas hourly space velocity (GHSV) of 120,000 mL g^{-1} h^{-1}. The correlations among the structures, acid properties and redox behaviors of the catalysts were tried to establish. The BET specific surface areas of the binary oxides were larger than those of the monadic ones. The sample with Ce/Nb (1:1) possessed special NbO_4 tetrahedral coordination. The surface acid sites were mainly provided by niobium oxide species. The Nb—OH bond was related to the Brønsted acid site and the Nb═O bond to the Lewis acid site. The abundance of surface adsorbed oxygen, the key factors for the catalytic behaviors, might arise from the short-range activation effect of niobium oxide species to cerium oxide species. In addition, water vapor only had a slight and reversible inhibition effect on the catalytic performance of the catalyst, and it might be a promising SCR catalyst for the practical application.

1. Introduction

Nitrogen oxides (NO_x), which mainly emitted from stationary and mobile sources, are major air pollutants because they can cause photochemical smog and acid rain. The selective catalytic reduction (SCR) of nitrogen oxides (NO_x) with ammonia has become an efficient technology for the abatement of NO_x from the exhausts of stationary and mobile sources [1]. Nowadays the TiO_2-anatase supported V_2O_5-WO_3 or V_2O_5-MoO_3 oxides have been commercialized for stationary applications. However, several problems have arisen during the industrial applications of the commercial catalysts, such as the trend to deactivate at higher temperatures, the high oxidation of SO_2 to SO_3 [2,3], the narrow operation temperature window of 300–400 °C and the formation of N_2O at high temperatures [4]. Therefore, many efforts have been made to develop vanadium-free catalyst systems.

Some transition metal oxides, such as MnO_x, CuO, Fe_2O_3 and CeO_2, have been found to be active for the SCR of NO with NH_3. Among them, cerium oxide (CeO_2) has been extensively investigated due to (i) the excellent oxygen storage capacities (OSC) on the basis of the redox behavior between Ce^{3+} and Ce^{4+}; (ii) the relatively easy formation of labile oxygen vacancies and the high mobility of bulk oxygen species [5]. CeO_2 has been used as a key component in three-way catalysts (TWC) for the gasoline engine emission control [6]. Furthermore, CeO_2 is thought to be a good promoter for the vanadium-based catalysts [7,8]. In addition, cerium-exchanged mordenite [9], MnO_x-CeO_2 [10,11], WO_3/CeO_2-ZrO_2 [12], CeO_2/TiO_2 [13–16], CeO_2/Al_2O_3 [17] and CeO_2-WO_3 [18,19] systems have also been investigated and found to be active for the catalytic reduction of NO.

Niobium compounds have attracted much attention as catalysts for various reactions [20–22]. The unique acid properties of niobium oxide make it suitable for the SCR reaction. Nb_2O_5/FeO_x [23], V_2O_5-Nb_2O_5/TiO_2 [24], MnO_x-Nb_2O_5-CeO_2 [25], Ag-Nb_2O_5/Al_2O_3 [26] and V_2O_5-Nb_2O_5-Sb_2O_5/TiO_2 [27] systems have been studied for the catalytic removal of NO.

In the SCR reaction, a dual-site mechanism, including an acid site and a redox site, has been proposed [28]. So the combination of the Nb_2O_5 acid properties and the redox behaviors of CeO_2 may result in good SCR performance. CeO_2-Nb_2O_5 system has been reported as a promising multi-purpose catalyst for the SCR of NO_x, urea hydrolysis and soot oxidation in diesel exhaust [29]. However, the performance of NH_3-SCR of NO_x on this kind of metal oxide is seldom investigated, and the information including the structure-activity relationship and the active sites are crucial for

* Corresponding author. Tel.: +86 571 87951335.
** Corresponding author. Tel.: +86 10 62771093.
E-mail addresses: xgao1@zju.edu.cn (X. Gao), lijunhua@tsinghua.edu.cn (J. Li).

0926-3373/$ – see front matter © 2013 Elsevier B.V. All rights reserved.
http://dx.doi.org/10.1016/j.apcatb.2013.05.035

the practical application. Therefore, it is necessary to study the correlations among the catalytic performances, the structures and the acid/redox properties of the binary systems. In this work, the structure properties are characterized by N_2 adsorption, X-ray diffraction (XRD) and Raman spectra. Then the acid properties are characterized by ammonia temperature programmed desorption (NH_3-TPD) and *in situ* diffuse reflectance Fourier transform spectroscopy (*in situ* DRIFTS) of NH_3 adsorption. Moreover, X-ray photoelectron spectroscopy (XPS) and hydrogen temperature programmed reduction (H_2-TPR) are used for the evaluation of redox behaviors of the catalysts.

2. Experimental

2.1. Catalyst preparation

The cerium-niobium mixed oxides were prepared by co-precipitation method. Desired amount of niobium chloride was dissolved in methanol and cerium nitrate in deionized water, respectively. These two kinds of solutions were mixed together and added into an excess of ammonia solution with continuous stirring. Afterwards, the precipitates were collected by filtration for several times until no residue Cl^- (detected by $AgNO_3$ solution), dried at 120 °C overnight and calcined at 500 °C for 5 h under air conditions. The catalysts were crushed and sieved to 40–60 meshes for activity tests. The molar ratios of Ce/Nb were 1/3, 1/1, and 3/1. The single oxides, namely Nb_2O_5 and CeO_2, were prepared by similar precipitation method.

2.2. Catalytic performance tests

The catalytic performance tests for all the catalysts were performed in a fixed-bed quartz reactor. 0.1 g granular catalyst (40–60 mesh) was used for evaluation. The feed gas mixture contained 500 ppm NO, 500 ppm NH_3, 5% O_2, 4.5% H_2O (when used) and N_2 as the balance. The total flow rate of the feed gas was 200 mL min^{-1}, corresponding to a gas hourly space velocity (GHSV) of 120, 000 mL g^{-1} h^{-1}. The concentrations of the inlet and outlet gases were continuously monitored by an FTIR spectrometer (MKS, MultiGas 2030HS). All the experimental data were recorded when the steady-state reaction was reached after 30 min at each temperature. NO conversion (X), N_2 selectivity (S) and the pseudo-first order rate constant (k) are calculated as follows [30,31]:

$$X = \left(1 - \frac{[NO]_{out}}{[NO]_{in}}\right) \times 100\% \quad (1)$$

$$S = \left(1 - \frac{2[N_2O]_{out} + [NO_2]_{out}}{[NO]_{in} + [NH_3]_{in}}\right) \times 100\% \quad (2)$$

$$k = -\frac{F}{W} \ln(1 - X) \quad (3)$$

where $[NO]_{in}$ and $[NO]_{out}$ represented the inlet and outlet concentrations of gaseous NO, respectively; $[N_2O]_{out}$ and $[NO_2]_{out}$ were the outlet concentrations of N_2O and NO_2; F was the total flow rate and W the weight of the catalyst.

2.3. Physicochemical characterizations

N_2 adsorption–desorption experiments were performed using a Quantachrome Autosorb-1 instrument at liquid N_2 temperature (−196 °C). The samples were outgassed at 300 °C for 4 h before N_2 adsorption. The specific surface areas were determined by the Brunauer–Emmett–Teller (BET) equation at P/P_0 in the range of 0.05–0.35. Pore size distributions and average pore diameters were determined by the Barrett–Joyner–Halenda (BJH) method using the desorption branches in 0.35–0.95 partial pressure range.

Powder X-ray diffraction (XRD) patterns were measured on an X-ray diffractometer (Rigaku, D/max-2200, Japan) equipped with a Cu Kα radiation source (λ = 0.15405 nm, 40 mV and 200 mA). The scanning range was from 10 to 80° at a step of 10° min^{-1} with the step size of 0.02°.

The structure of the catalysts were studied by the micro-Raman spectroscopy (Renisaw, InVia) under the 532 nm excitation laser light.

Temperature programmed desorption of ammonia (NH_3-TPD) was carried out on the Chemisorb 2007 TPx using FTIR spectrometer (MKS, MultiGas 2030HS) for detecting different nitrogen-containing species including NH_3, N_2O and NO. Prior to the experiment, the samples were pretreated at 350 °C for 1 h. Then the samples were cooled down to 50 °C and saturated with NH_3 until adsorption equilibrium was reached, followed by flushing with N_2 at 100 °C to avoid physisorption of NH_3. The NH_3-saturated samples were then heated from 100 °C to 500 °C at a rate of 10 °C min^{-1}.

In situ diffuse reflectance infrared Fourier transform spectroscopy (*in situ* DRIFTS) experiments of NH_3 adsorption were performed on an Fourier transform infrared spectrometer (FTIR, Nicolet NEXUS 6700), equipped with an MCT/A detector. The samples were pretreated at 350 °C for 1 h in N_2 with a flow of 100 mL min^{-1} before each experiment. All the IR spectra were recorded by collecting 32 scans with a resolution of 4 cm^{-1}.

X-ray photoelectron spectroscopy (XPS) analysis was performed on an ESCALab220i-XL electron spectrometer from VG Scientific using 300 W Mg Ka radiation. The base pressure was approximately 3×10^{-9} mbar. The binding energies of all the elements were referenced to the C 1 s line at 284.8 eV from carbon impurities.

Temperature programmed reduction of hydrogen (H_2-TPR) experiments were carried out on a chemisorption analyzer (Micromeritics, ChemiSorb 2720 TPx). The samples were pretreated at 350 °C for 1 h before each experiment. Then the samples were cooled down to room temperature in a flow of N_2. The reduction of the samples was initiated from room temperature to 1000 °C, with a mixture of 10% H_2/Ar (50 mL min^{-1}) at a rate of 10 °C min^{-1}. The consumption of H_2 was continuously monitored using a thermal conductivity detector (TCD).

3. Results and discussion

3.1. Catalytic performances

The catalytic activities of the catalysts with different Ce/Nb ratios (0/1, 1/3, 1/1, 3/1, 1/0) were tested in the temperature range of 150 °C–450 °C and the results are shown in Fig. 1. Single metal oxides (CeO_2 and Nb_2O_5) showed negligible NO conversion. Upon addition of CeO_2 to Nb_2O_5 (Ce/Nb = 1/3), dramatic increase in the SCR activity within the whole temperature range was observed. Further increasing the relative amount of CeO_2 (Ce/Nb = 1/1), the NO conversion below 250 °C increased but the one above 400 °C decreased. With the Ce/Nb being 3/1, the operation temperature window shifted slightly toward higher temperatures. Considering the N_2 selectivity for the binary catalysts, similar tendencies with NO conversion at higher temperatures were obtained, as shown in Fig. 2. As for CeO_2, quite amount of N_2O was formed at higher temperatures. The addition of Nb_2O_5 to CeO_2 resulted in the enhancement of N_2 selectivity, in accordance with previous study [25,27]. The results of catalytic activity and selectivity imply that strong interactions exist between Ce and Nb oxide species for the SCR of NO with NH_3. Various characterizations were carried out to illustrate the physicochemical properties of the catalysts and the correlations between structures and catalytic activities.

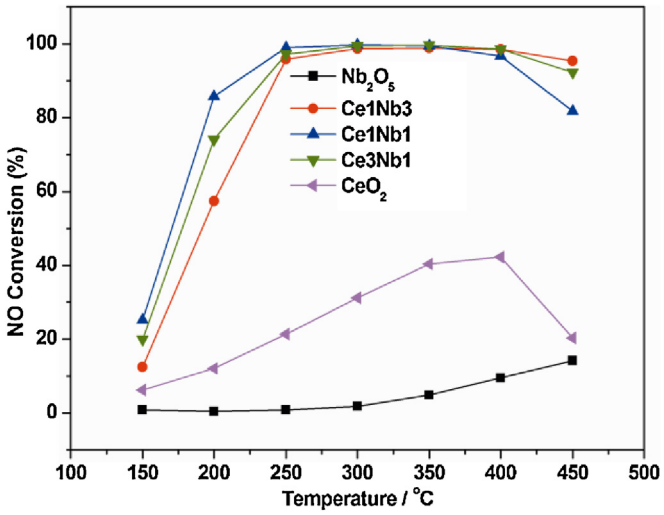

Fig. 1. SCR performances over CexNby serial catalysts. Reaction condition: $[NH_3] = [NO] = 500$ ppm, $[O_2] = 5\%$, total flow rate = 200 mL min^{-1}, catalyst mass = 0.1 g, GHSV = 120,000 mL g^{-1} h^{-1}.

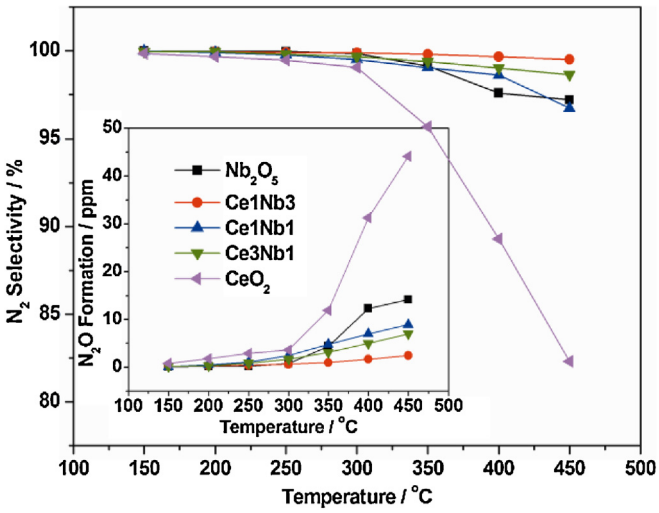

Fig. 2. N_2 selectivity and N_2O formation over CexNby serial catalysts. Reaction condition: $[NH_3] = [NO] = 500$ ppm, $[O_2] = 5\%$, total flow rate = 200 mL min^{-1}, catalyst mass = 0.1 g, GHSV = 120,000 mL g^{-1} h^{-1}.

3.2. Physicochemical characterizations

3.2.1. Structures of the samples

The N_2 adsorption–desorption isotherms of the samples are shown in Fig. 3(A). All the catalysts exhibited typical type IV isotherms, which is always associated with capillary condensation in mesopores [32]. As for CeO_2, it was likely that the hysteresis loop was demonstrated to be H1 type. Upon addition of Nb_2O_5 to CeO_2, typically Ce1Nb1 and Ce1Nb3, the hysteresis loops shifted to H2 type, indicative of the possible formation of an ink-bottle-shaped structure, which may enlarge the inner surface area. Besides, the pore size distributions of Ce1Nb1, Ce1Nb3 and Nb_2O_5, as can be seen in Fig. 3(B), were rather narrow. Broad pore size distributions could be obtained for CeO_2 and Ce3Nb1. The BET specific surface areas (S_{BET}), total pore volumes (V_p) and average pore diameters (D_p) of all the samples are summarized in Table 1 based on the calculation from the isotherms. Compared with the CeO_2 and Nb_2O_5, the binary oxides have larger S_{BET} which could provide more surface active sites for the SCR reaction. As a consequence, the combination of CeO_2 and Nb_2O_5 can result in the variations of the physical structures which are beneficial for the reaction.

The XRD patterns of the catalysts are presented in Fig. 4. All the reflections of CeO_2 provide typical diffraction patterns for the cerianite (PDF-ICDD 43-1002). Similar pattern is observed for Ce3Nb1, while a slight shift toward higher 2θ value can be observed, which might be attributed to the incorporation of Nb_2O_5 into CeO_2 lattice. With the ratios of Ce/Nb being 1/1 and 1/3, broad diffraction peaks can be obtained, indicative of amorphous structures. As for Nb_2O_5, the reflections provide diffraction patterns for niobium oxide (PDF-ICDD 27-1003).

The Raman spectra of the samples are shown in Fig. 5. The spectrum of CeO_2 is solely presented in Fig. 5(A) due to its strong intensity which may make weaker peaks unobvious if the spectra of all the samples were put together. The bands at 252, 463, 446

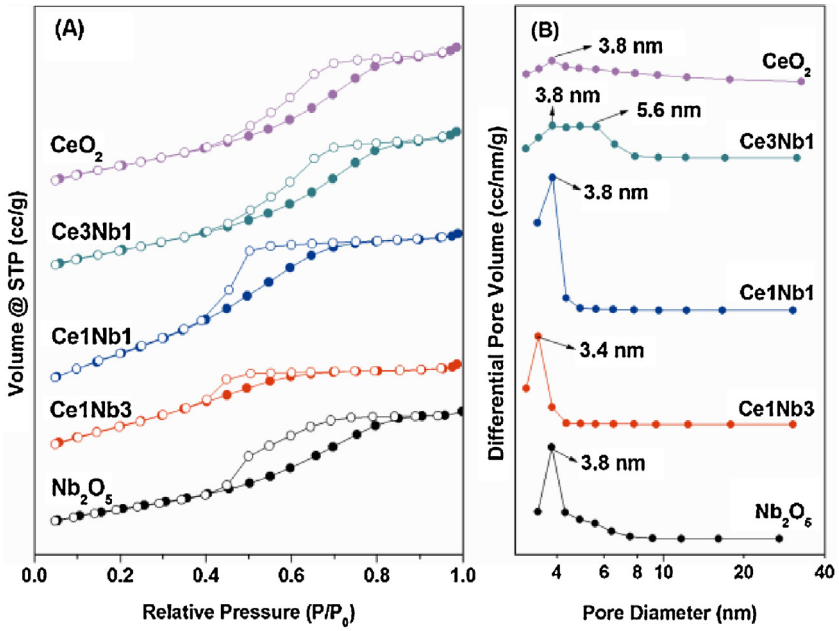

Fig. 3. N_2 adsorption results of the CexNby serial catalysts. (A) N_2 adsorption–desorption isotherms; (B) pore size distributions.

Table 1
N_2 adsorption results, NH_3 desorption amount and XPS results of the CexNby serial catalysts.

Sample	S_{BET} ($m^2\ g^{-1}$)	V_p ($cc\ g^{-1}$)	D_p (nm)	Acidity ($\mu mol\ g^{-1}$)	$Ce^{3+}/(Ce^{3+}+Ce^{4+})$ %
Nb_2O_5	96	0.131	5.4	99	–
Ce1Nb3	134	0.112	3.4	143	0.28
Ce1Nb1	179	0.186	4.1	182	0.22
Ce3Nb1	110	0.156	5.6	114	0.16
CeO_2	105	0.179	6.8	38	–

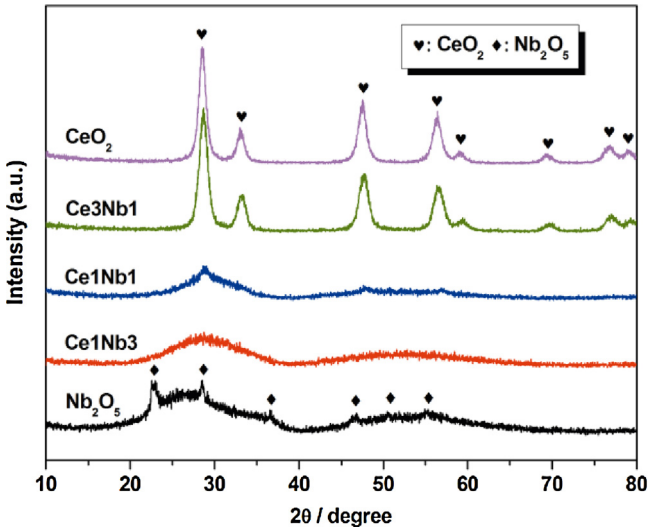

Fig. 4. XRD patterns of the CexNby serial catalysts.

and 598 cm^{-1} can be associated with the cerium oxide species and the bands at 309, 620, 664, 796, 800, 876, 939 and 975 cm^{-1} with niobia species. The attributions of the bands for niobium species are listed in Figs. 5(C)–(E), according to the literature [33]. As shown in Fig. 5(A), a sharp peak centered at 463 cm^{-1} was observed, which is attributed to the F_{2g} Raman-active mode characteristic of the fluorite structure of ceria [34]. In addition, it also shows two week bands at ~252 cm^{-1} and ~598 cm^{-1}, which can be ascribed to the normally Raman inactive (IR active) transverse and longitudinal optical phonon modes at the Brillouin zone center, respectively [34,35]. As for Ce3Nb1, peaks at ~252 and 463 cm^{-1} can also be observed. These results are in well accordance with the XRD patterns, in which similar cerianite structure are obtained for CeO_2 and Ce3Nb1. In addition, a broad band at ~800 cm^{-1}, and a small shoulder at ~975 cm^{-1}, as shown in the inset of Fig. 5(B), are presented, indicative of the existence of highly distorted octahedrally and tetrahedrally coordinated niobium oxide compounds. The band at ~588 cm^{-1} may arise from the overlapping of peaks for ceria or niobia species. In the case of Ce1Nb1, the peak at 446 cm^{-1} shows an obvious shift toward lower wavenumber, which indicates a decrease in the cerium-oxygen bond order, corresponding to a longer bond distance. A remarkable decrease in intensity is also shown for this peak. The Raman bands appearing at 309 and 796 cm^{-1} are due to the Nb—O symmetric modes of the NbO_4 tetrahedral structure, suggesting that the structure of niobium species is mainly tetrahedrally coordinated niobium oxide compound. For Ce1Nb3 and Nb_2O_5, several bands at 620, 664, 876 and 939 cm^{-1} are presented, suggesting the structures of niobium species in these niobium-rich samples are mainly octahedrally coordinated niobium oxide compound.

It has been reported that the tetrahedral NbO_4 structure are rarely found in niobium oxide compounds due to the large size of Nb^{5+} which may not fit into an oxygen-anion tetrahedron [36]. However, some rare-earth $ANbO_4$ (A = Y, Yb, Sm and La) compounds have been reported to possess NbO_4 tetrahedral coordination [36–38]. Cerium is a well known rare-earth element. So the tetrahedral coordination of niobium oxide compounds is reasonable in cerium-niobium mixed oxides. It should be noted that the NbO_4

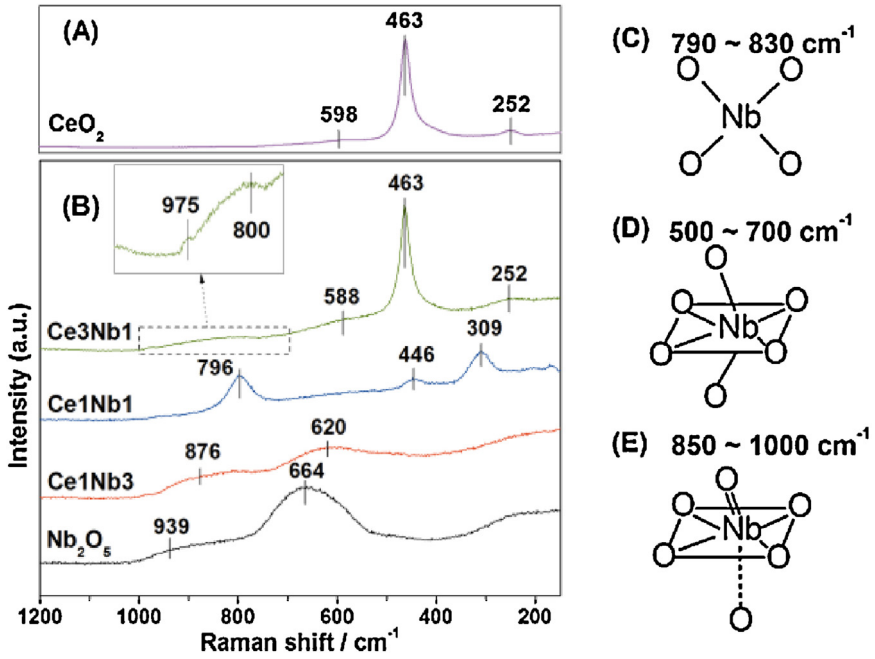

Fig. 5. Raman spectra of the CexNby serial catalysts.

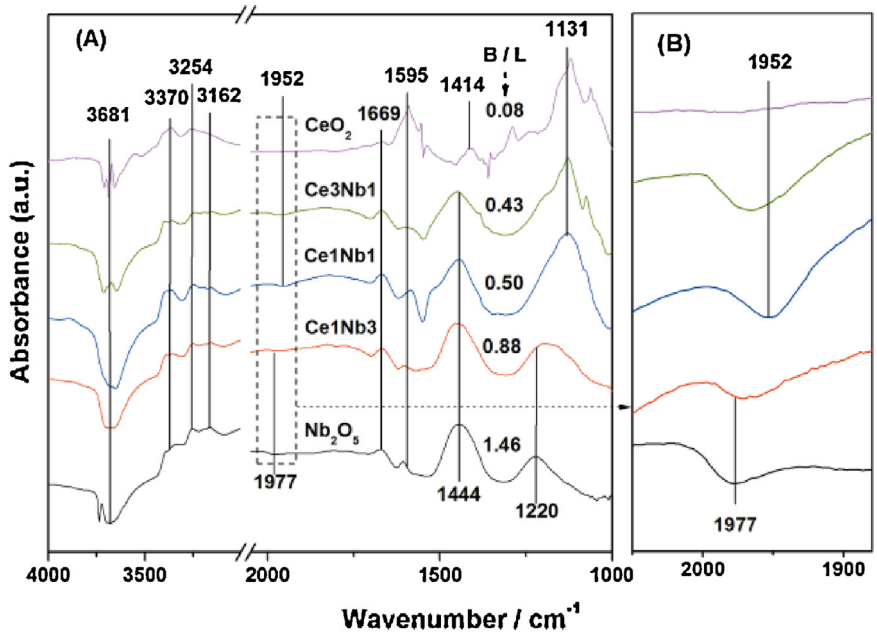

Fig. 6. *In situ* DRIFTS of NH_3 adsorption at 50 °C over Ce*x*Nb*y* serial catalysts.

tetrahedral coordination is the most obvious in Ce1Nb1, compared with other samples. In addition, the Raman band of Ce1Nb1 at 446 cm^{-1} shows obvious shift toward lower wavenumber, compared with the bands of Ce3Nb1 and CeO_2, suggesting a lower cerium-oxygen bond order as discussed above. The differences in the structures of the samples can result in some different properties, which may directly affect the catalytic performances.

3.2.2. Acid properties of the samples

The NH_3-TPD was performed to investigate the surface acidities of the samples and the results are shown in Table 1. CeO_2 desorbed very small amount of NH_3. Upon addition of Nb_2O_5, obvious increase in the desorbed amount of NH_3 can be observed, suggesting that Nb_2O_5 could help to adsorb NH_3 due to its acid properties.

In situ DRIFTS of NH_3 adsorption on these samples was performed at 50 °C and the results are shown in Fig. 6(A). The bands centered around 1595 cm^{-1} and 1131, 1220 cm^{-1} can be attributed to the asymmetric and symmetric bending vibrations of ammonia species coordinated on Lewis acid sites [39]. The bands centered around 1414, 1444 and 1669 cm^{-1} can be ascribed to the asymmetric and symmetric bending vibrations of ionic NH_4^+ species linked to Brønsted acid sites [40]. The bands at 3162, 3254 and 3370 cm^{-1} are assigned to the N—H stretching vibration modes [39]. The negative bands around 3681 cm^{-1} can be ascribed to the consumption of surface hydroxyl groups [41]. The ratios of the integrated peak areas of 1414, 1444 and 1131, 1220 cm^{-1}, which can be regarded as the characteristic bands for ammonia species linked to Brønsted and Lewis acid sites, are listed in Fig. 6(A). We can easily find that the introduction of niobium oxides to cerium oxides significantly affects the acid site distribution of the catalysts. Brønsted acid sites are associated closely with the relative amount of niobium oxide species. It should be pointed out that several negative bands around 1952 and 1977 cm^{-1}, as magnified in Fig. 6(B), can be observed for the Nb-containing samples. These bands can be ascribed to the stretching mode of Nb=O in the overtone region [42]. The Nb=O stretching mode in the fundamental region (at ~980 cm^{-1}, not shown here) was overlapped by the noise so that it could not be clearly observed. The negative Nb=O overtones indicate the consumption of Nb=O bond during the process of NH_3 adsorption. That is to say, the Nb=O bond can act as an acid site for the adsorption of NH_3.

It has been reported that Nb=O bonds might play the role as either Brønsted acid sites [43] or Lewis acid sites [22]. In order to illustrate the role of Nb=O bonds in the process of NH_3 adsorption, we selected Ce1Nb1 to investigate the NH_3 adsorption behaviors at different temperatures and the result is shown in Fig. 7(A). As is stated above, the bands around 1442 and 1136, 1195 cm^{-1} can be regarded as characteristic bands for NH_3 adsorbed on Brønsted acid sites and Lewis acid sites, respectively. The negative bands centered at 1952 cm^{-1} are attributed to the Nb=O overtones. It can be seen that the intensities of the bands at 1442 cm^{-1} diminished quickly with the increase of temperature and vanished at 250 °C. While the negative bands at 1952 cm^{-1} and the ones at 1136 or 1195 cm^{-1}, disappeared at 350 °C. As shown in Fig. 7(B) and (C), the intensities of the bands at 1952 cm^{-1} and 1136, 1195 cm^{-1} decreased and vanished simultaneously, indicating that the Nb=O bond is responsible for NH_3 bounded at Lewis acid sites. The surface hydroxyl groups (Nb—OH), which are presented as the negative bands around 3681 cm^{-1}, are responsible for the Brønsted acid sites.

A large number of investigations have been carried out to illustrate the role of the acid sites. It is claimed that both Brønsted acid and Lewis acid mechanisms can contribute to the reaction [39,44]. As shown in Fig. 7, NH_3 adsorbed on Brønsted acid site has less thermal stability. Ionic NH_4^+ species linked to Brønsted acid site can hardly exist at temperatures higher than 250 °C, which means that the Brønsted acid site may contribute to the reaction only at relatively low temperatures. In contrast, NH_3 species coordinated on Lewis acid site have better thermal stability than NH_4^+ species. So it is supposed that NH_3 adsorbed Lewis acid site may contribute to the reaction at both low and high temperatures.

As a consequence, the introduction of niobium oxide species to cerium oxide species leads to an obvious enhancement of the total acidity of the samples. Both Brønsted acid site and Lewis acid site can be brought by niobium oxides. The Nb—OH bond is responsible for Brønsted acid site and Nb=O bond for Lewis acid site. At low temperatures, both Brønsted acid site and Lewis acid site may contribute to the reaction. Only Lewis acid site is responsible for the reaction at high temperatures.

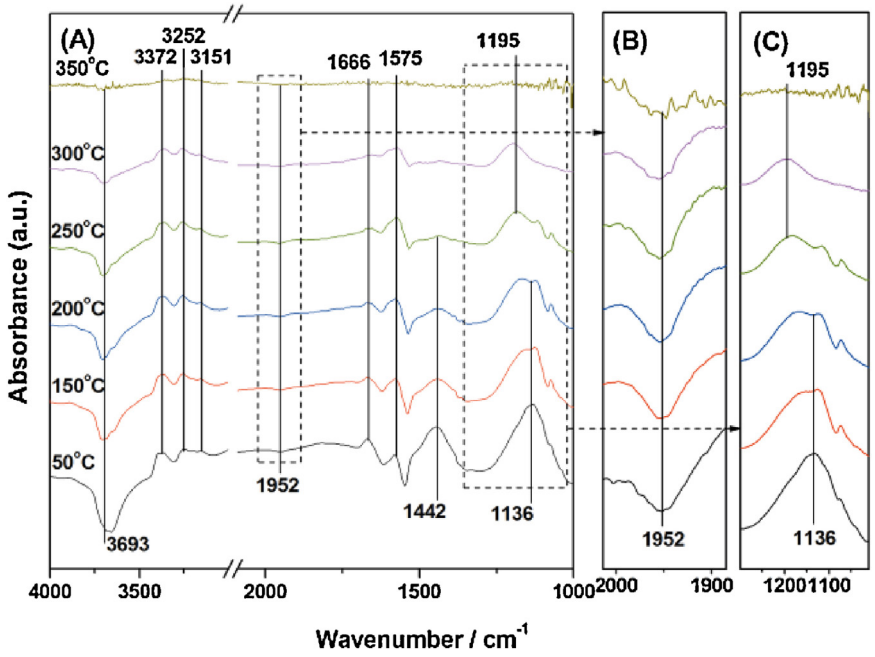

Fig. 7. *In situ* DRIFTS of NH_3 adsorption at different temperatures over Ce1Nb1 catalyst.

3.2.3. Redox properties of the samples

XPS technique was used to obtain a better understanding of the chemical states of all the elements in the cerium-niobium mixed oxides. Fig. 8(A) shows the XPS spectra of Ce 3d for the binary samples. Eight peaks can be obtained by fitting the curves. As is reported in the literature [45], the peaks centered at ~886 and 904 eV can be assigned to Ce^{3+} and others to Ce^{4+}. Fig. 8(B) shows the XPS spectra of Nb 3d for the samples. It can be determined that the peaks centered at ~207 eV could be assigned to the Nb^{5+} species [46]. The XPS spectra of O 1s are shown in Fig. 8(C). The peaks at 529.8–530.2 eV are attributed to lattice oxygen (O^{2-}) (denoted as O_β) and the ones at 531.2–531.6 eV can be assigned to the surface-adsorbed oxygen (denoted as O_α). The relative concentration ratios of $O_\alpha/(O_\alpha+O_\beta)$ for each sample are also calculated and the results are shown in Fig. 8(C). As is presented in Fig. 8(D), good correlation can be observed between the relative concentration ratios of $O_\alpha/(O_\alpha+O_\beta)$ and the pseudo-first order rate constant (k) at 150 °C, indicating that the relative concentration ratios of surface adsorbed oxygen are directly related to the catalytic performances of the catalysts at low temperatures.

The H_2-TPR profiles of the catalysts are shown in Fig. 9(A). The reduction of Nb_2O_5 starts at ~800 °C, which is responsible

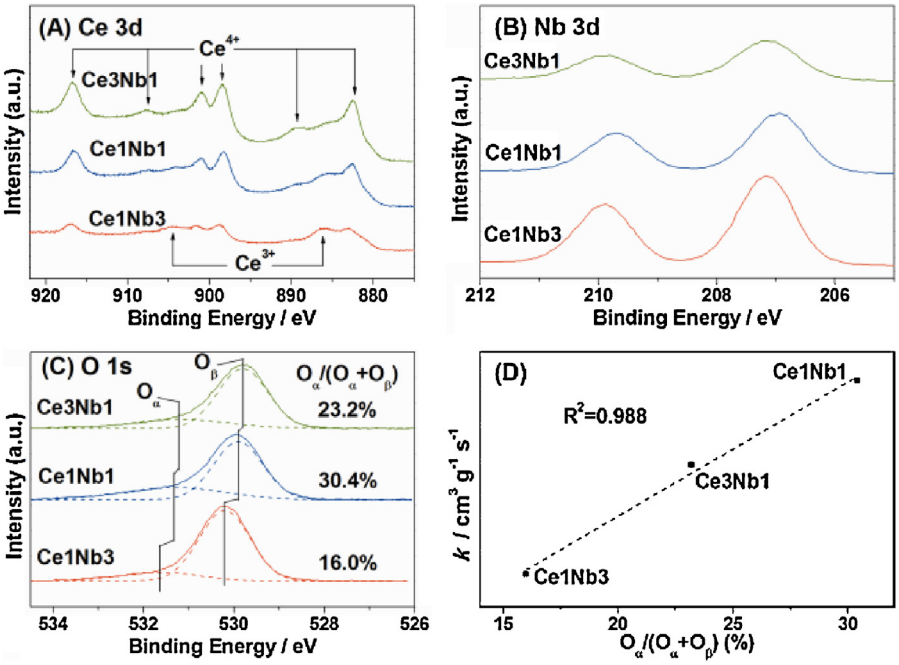

Fig. 8. XPS spectra of the CexNby binary catalysts over the spectral regions of (A) Ce 3d; (B) Nb 3d; (C) O 1s. (D) Correlations between the relative concentrations of surface-adsorbed oxygen ($O_\alpha/(O_\alpha+O_\beta)$) and the pseudo-first order rate constant (k) at 150 °C.

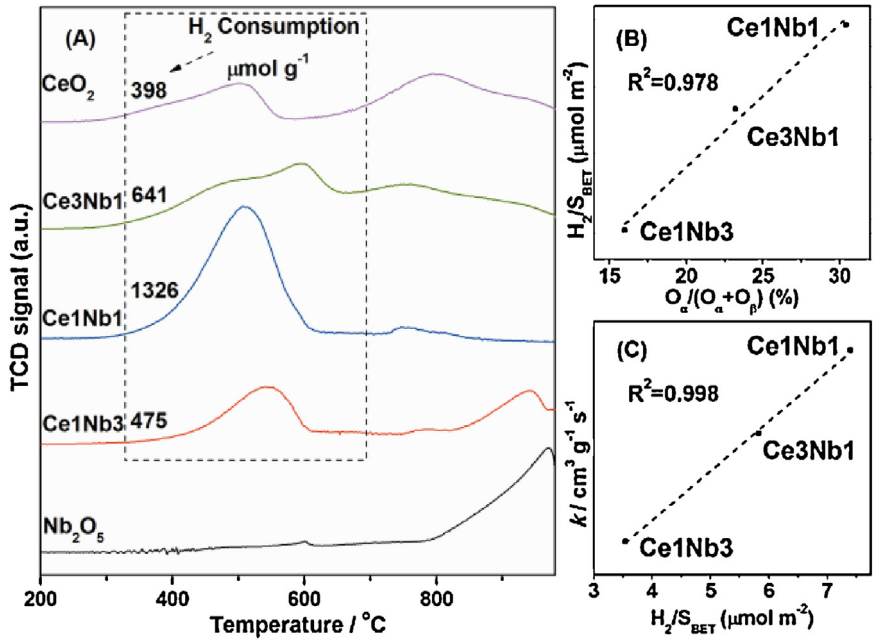

Fig. 9. (A) H_2-TPR profiles of the Ce*x*Nb*y* serial catalysts. (B) Correlations between the $O_\alpha/(O_\alpha + O_\beta)$ and H_2/S_{BET}. (C) Correlations between the H_2/S_{BET} and k at 150 °C.

for the reduction of bulk Nb_2O_5 to bulk Nb_2O_4 [47,48]. As for the cerium-containing samples, it is obvious that at least one reduction peak occurs before 700 °C. In the case of cerium oxide species, the reduction of bulk oxygen usually takes place above 700 °C and the peaks below 700 °C can be associated with the reduction of surface capping oxygen [6], which is always responsible for the catalytic reaction. The total H_2 consumption for the peaks below 700 °C are calculated and results are listed in the inset of Fig. 9(A). Due to the fact that the H_2 consumption for the peaks below 700 °C was relevant to the BET surface area [6], we calculated the H_2 consumption (below 700 °C) per specific surface area (H_2/S_{BET}). Good correlations between the H_2/S_{BET} and relative concentration ratios of $O_\alpha/(O_\alpha + O_\beta)$ for the binary samples can be observed, as shown in Fig. 9(B), confirming that the reduction peaks below 700 °C are indeed associated with the reduction of surface capping oxygen. Furthermore, as can be seen in Fig. 9(C), good correlation can also be observed between the H_2/S_{BET} and k at 150 °C, suggesting again that the concentrations of surface adsorbed oxygen act as key factors for the redox properties as well as the catalytic behaviors of the binary oxides at low temperatures.

The surface active oxygen is related to the catalytic activity, and it is crucial to make clear the origin of them. Firstly, ceria itself has a certain amount of surface active oxygen while niobia almost has none, according to the H_2-TPR results. When doped into CeO_2, Nb remains four electrons available for making bonds, just like the Ce^{4+} it substituted. Moreover, the excess one electron is donated to the adjacent Ce^{4+}, which is then reduced to be Ce^{3+} [49,50]. So we can deduce that the relative amount of Ce^{3+} will increase with the increase of Nb/Ce ratio since the more Nb/Ce ratio, the more opportunities Ce may linked to Nb to form bond like Ce-O-Nb, thus generating Ce^{3+}. This claim is confirmed by calculating the relative amount of $Ce^{3+}/(Ce^{3+} + Ce^{4+})$ based on the XPS results in Table 1. Meanwhile the presence of Ce^{3+} is important to the chemisorbed oxygen on the surface because Ce^{3+} could lead to charge imbalance, oxygen vacancies and unsaturated chemical bonds [19]. So the effect of Nb is to activate the oxygen around ceria, not to provide additional active oxygen. In addition, this activation effect is only a short-range effect, i.e., only the oxygen atoms in ceria next to Nb can be affected [50]. As a result, the surface active oxygen can be devided into two categories: the one activated by Nb (denoted as OCN in short) and the one owned by ceria itself (denoted as OC). The oxygen possessed by niobia itself (denoted as ON) is relatively inert. Considering the three binary samples, we can suppose that Ce3Nb1 has a small amount of OCN and a certain amount of OC, Ce1Nb1 a large amount of OCN whereas Ce1Nb3 a small amount of OCN. The above hypothesis seems reasonable considering the molar ratio of Ce/Nb. In addition, the number of the peaks below 700 °C in the H_2-TPR profiles also supports this claim. Meanwhile, considering the structures of the samples, we can find that both Ce1Nb1 and Ce3Nb1 possess the tetrahedral NbO_4 structure, which can be regarded as monomeric unit, while the octahedrally coordinated niobium oxide species, appeared at niobium-rich catalysts, as polymerized one [42]. It seems reasonable that the monomeric niobium oxide species have more opportunities to bond to cerium oxide species than the polymerized one. Consequently, the introduction of niobium oxide species has an obvious effect on the adjacent

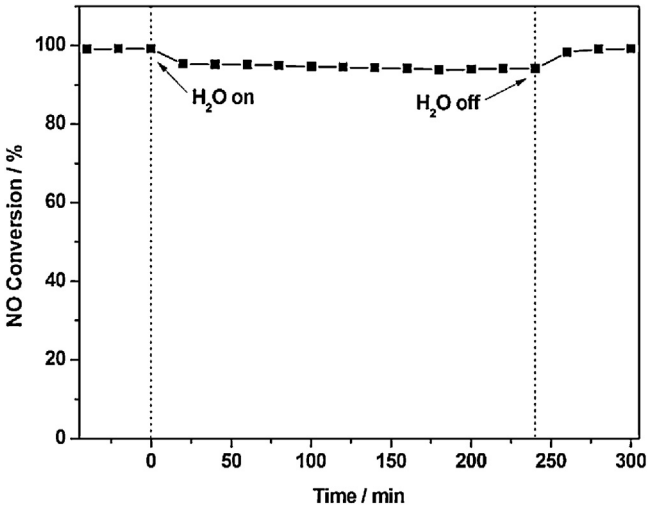

Fig. 10. Effect of 4.5% H_2O on the SCR raction over Ce1Nb1 catalyst at 300 °C at a GHSV of 120, 000 mL g^{-1} h^{-1}.

cerium species, altering the redox properties and enhancing the catalytic performances of the catalysts.

3.2.4. Effect of H_2O

Water vapor remains one of the typical components in the exhaust gases and always significantly influences the catalytic activity. It is important to know the catalytic performance of the catalyst with H_2O in the feed. Therefore, the effect of water vapor on the SCR reaction over Ce1Nb1 catalyst at 300 °C was investigated and the result is shown in Fig. 10. During the test for 4 h, the ratio of NO conversion slightly decreased and remained above 93%. This result indicates that water vapor inhibits the catalytic activity slightly at 300 °C, possibility due to the competitive adsorption with NH_3 [51]. Moreover, the catalytic activity fully recovered after removal of water vapor, suggesting that the inhibition effect is reversible.

4. Conclusions

A series of cerium-niobium binary oxide catalysts, synthesized using co-precipitation method, showed excellent catalytic activity and selectivity for the selective catalytic reduction of NO with NH_3. The correlations among the catalytic performances, the structures and the acid/redox properties were investigated. Several conclusions can be drawn as follows:

(1) The combination of cerium oxide and niobium oxide results in larger specific surface areas compared with the single metal oxides, which can provide more active sites for the reaction. Moreover, this combination leads to variations in the structures. The niobium oxide species in Ce1Nb1 possesses the unusual tetrahedral NbO_4 structure, which may affect the redox properties of the catalysts.
(2) Niobium oxide species in the mixed oxides clearly enhanced the total acidity of the catalysts, especially the amount of Brønsted acid site. The Nb—OH bond can serve as the Brønsted acid site and the Nb═O bond as the Lewis acid site. At low temperatures, both Brønsted acid site and Lewis acid site may contribute to the reaction. While only Lewis acid site is responsible for the reaction at high temperatures.
(3) The relative concentration ratios of surface adsorbed oxygen play a key role in the SCR reaction and the amount of surface adsorbed oxygen is related to the short-range activation effect caused by niobium species, which may affect the chemical environmental of the adjacent cerium species, resulting in an abundance of surface adsorbed oxygen, thus giving rise to the higher catalytic performances at low temperatures.

Acknowledgements

The authors gratefully acknowledge the financial support from the National Science Foundation for Distinguished Young Scholars of China (No. 51125025) and the National High-Tech Research and Development (863) Program of China (No. 2012AA062506).

References

[1] G. Busca, L. Lietti, G. Ramis, F. Berti, Applied Catalysis B: Environmental 18 (1998) 1–36.
[2] J.P. Dunn, P.R. Koppula, H.G. Stenger, I.E. Wachs, Applied Catalysis B: Environmental 19 (1998) 103–117.
[3] J.P. Dunn, H.G. Stenger, I.E. Wachs, Journal of Catalysis 181 (1999) 233–243.
[4] M. Yates, J.A. Martin, M.A. Martin-Luengo, S. Suarez, J. Blanco, Catalysis Today 107–08 (2005) 120–125.
[5] B.M. Reddy, A. Khan, Y. Yamada, T. Kobayashi, S. Loridant, J.C. Volta, Journal of Physical Chemistry B 107 (2003) 5162–5167.
[6] A. Trovarelli, Catalysis Reviews–Science and Engineering 38 (1996) 439–520.
[7] S.S.R. Putluru, A. Riisager, R. Fehrmann, Catalysis Letters 133 (2009) 370–375.
[8] L. Chen, J.H. Li, M.F. Ge, Journal of Physical Chemistry C 113 (2009) 21177–21184.
[9] E. Ito, R.J. Hultermans, P.M. Lugt, M.H.W. Burgers, M.S. Rigutto, H. Vanbekkum, C.M. Vandenbleek, Applied Catalysis B: Environmental 4 (1994) 95–104.
[10] M. Casapu, O. Kroecher, M. Elsener, Applied Catalysis B: Environmental 88 (2009) 413–419.
[11] G.S. Qi, R.T. Yang, Chemical Communications (2003) 848–849.
[12] Y. Li, H. Cheng, D.Y. Li, Y.S. Qin, Y.M. Xie, S.D. Wang, Chemical Communications (2008) 1470–1472.
[13] W.Q. Xu, Y.B. Yu, C.B. Zhang, H. He, Catalysis Communications 9 (2008) 1453–1457.
[14] X. Gao, Y. Jiang, Y. Zhong, Z.Y. Luo, K.F. Cen, Journal of Hazardous Materials 174 (2010) 734–739.
[15] X. Gao, Y. Jiang, Y.C. Fu, Y. Zhong, Z.Y. Luo, K.F. Cen, Catalysis Communications 11 (2009) 465–469.
[16] W.P. Shan, F.D. Liu, H. He, X.Y. Shi, C.B. Zhang, ChemCatChem 3 (2011) 1286–1289.
[17] Y.S. Shen, S.M. Zhu, T. Qiu, S.B. Shen, Catalysis Communications 11 (2009) 20–23.
[18] W.P. Shan, F.D. Liu, H. He, X.Y. Shi, C.B. Zhang, Chemical Communications 47 (2011) 8046–8048.
[19] L. Chen, J.H. Li, W. Ablikim, J. Wang, H.Z. Chang, L. Ma, J.Y. Xu, M.F. Ge, H. Arandiyan, Catalysis Letters 141 (2011) 1859–1864.
[20] K. Tanabe, S. Okazaki, Applied Catalysis A-General 133 (1995) 191–218.
[21] K. Tanabe, Catalysis Today 8 (1990) 1–11.
[22] I. Nowak, M. Ziolek, Chemical Reviews 99 (1999) 3603–3624.
[23] S. Okazaki, H. Kuroha, T. Okuyama, Chemistry Letters 14 (1985) 45–48.
[24] K.A. Vikulov, A. Andreini, E.K. Poels, A. Bliek, Catalysis Letters 25 (1994) 49–54.
[25] M. Casapu, O. Kroecher, M. Mehring, M. Nachtegaal, C. Borca, M. Harfouche, D. Grolimund, Journal of Physical Chemistry C 114 (2010) 9791–9801.
[26] C. Petitto, H.P. Mutin, G. Delahay, Chemical Communications 47 (2011) 10728–10730.
[27] X.S. Du, X. Gao, Y.C. Fu, F. Gao, Z.Y. Luo, K.F. Cen, Journal of Colloid and Interface Science 368 (2012) 406–412.
[28] N.Y. Topsoe, Science 265 (1994) 1217–1219.
[29] M. Casapu, A. Bernhard, D. Peitz, M. Mehring, M. Elsener, O. Kroecher, Applied Catalysis B: Environmental 103 (2011) 79–84.
[30] F.D. Liu, H. He, C.B. Zhang, Z.C. Feng, L.R. Zheng, Y.N. Xie, T.D. Hu, Applied Catalysis B: Environmental 96 (2010) 408–420.
[31] S.J. Yang, J.H. Li, C.Z. Wang, J.H. Chen, L. Ma, H.Z. Chang, L. Chen, Y. Peng, N.Q. Yan, Applied Catalysis B: Environmental 117 (2012) 73–80.
[32] K.S.W. Sing, D.H. Everett, R.A.W. Haul, L. Moscou, R.A. Pierotti, J. Rouquerol, T. Siemieniewska, Pure and Applied Chemistry 57 (1985) 603–619.
[33] J.M. Jehng, I.E. Wachs, Chemistry of Materials 3 (1991) 100–107.
[34] A. Martinez-Arias, M. Fernandez-Garcia, L.N. Salamanca, R.X. Valenzuela, J.C. Conesa, J. Soria, Journal of Physical Chemistry B 104 (2000) 4038–4046.
[35] J.Z. Shyu, W.H. Weber, H.S. Gandhi, Journal of Physical Chemistry 92 (1988) 4964–4970.
[36] G. Blasse, Journal of Solid State Chemistry 7 (1973) 169–171.
[37] H.P. Rooksby, E.A.D. White, Acta Crystallographica 16 (1963) 888–890.
[38] S. Yoshida, Y. Nishimura, T. Tanaka, H. Kanai, T. Funabiki, Catalysis Today 8 (1990) 67–75.
[39] L. Chen, J. Li, M. Ge, Environmental Science and Technology 44 (2010) 9590–9596.
[40] W.P. Shan, F.D. Liu, H. He, X.Y. Shi, C.B. Zhang, Applied Catalysis B: Environmental 115 (2012) 100–106.
[41] F.D. Liu, H. He, C.B. Zhang, W.P. Shan, X.Y. Shi, Catalysis Today 175 (2011) 18–25.
[42] L.J. Burcham, J. Datka, I.E. Wachs, Journal of Physical Chemistry B 103 (1999) 6015–6024.
[43] T. Onfroy, G. Clet, M. Houalla, Journal of Physical Chemistry B 109 (2005) 14588–14594.
[44] A. Vittadini, M. Casarin, A. Selloni, Journal of Physical Chemistry B 109 (2005) 1652–1655.
[45] X.S. Du, X. Gao, L.W. Cui, Y.C. Fu, Z.Y. Luo, K.F. Cen, Fuel 92 (2012) 49–55.
[46] C.D. Wagner, W.M. Riggs, L.E. Davis, J.F. Moulder, G.E. Muilenberg, Handbook of X-ray Photoelectron Spectroscopy, PerkinElmer, Minnesota, 1979.
[47] I.E. Wachs, L.E. Briand, J.M. Jehng, L. Burcham, X.T. Gao, Catalysis Today 57 (2000) 323–330.
[48] D. Stosic, S. Bennici, V. Rakic, A. Auroux, Catalysis Today 192 (2012) 160–168.
[49] E.W. McFarland, H. Metiu, Chemical Reviews (2013), http://dx.doi.org/10.1021/cr300418s.
[50] Z.P. Hu, H. Metiu, Journal of Physical Chemistry C 115 (2011) 17898–17909.
[51] M.D. Amiridis, I.E. Wachs, G. Deo, J.M. Jehng, D.S. Kim, Journal of Catalysis 161 (1996) 247–253.